Molecular Cell, Volume *81*

Supplemental Information

Protein Synthesis in the Developing Neocortex at Near-Atomic Resolution Reveals Ebp1-Mediated Neuronal Proteostasis at the 60S Tunnel Exit

Matthew L. Kraushar, Ferdinand Krupp, Dermot Harnett, Paul Turko, Mateusz C. Ambrozkiewicz, Thiemo Sprink, Koshi Imami, Manuel Günnigmann, Ulrike Zinnall, Carlos H. Vieira-Vieira, Theres Schaub, Agnieszka Münster-Wandowski, Jörg Bürger, Ekaterina Borisova, Hiroshi Yamamoto, Mladen-Roko Rasin, Uwe Ohler, Dieter Beule, Thorsten Mielke, Victor Tarabykin, Markus Landthaler, Günter Kramer, Imre Vida, Matthias Selbach, and Christian M.T. Spahn

Supplementary Figure 1

Kraushar ML, *et al.*

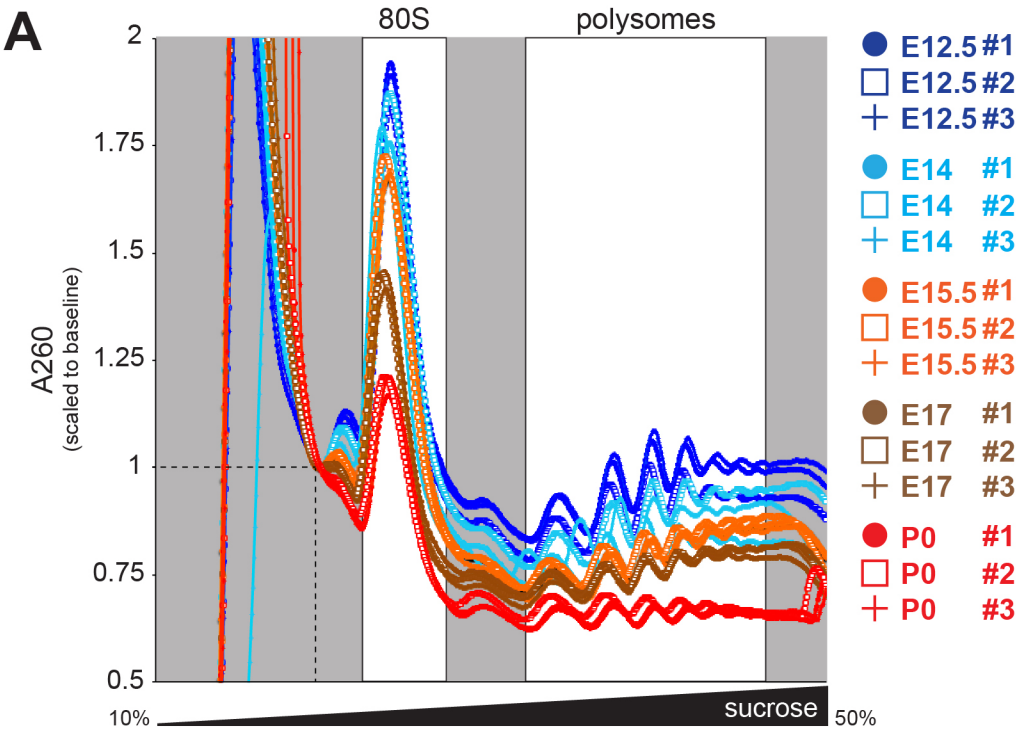

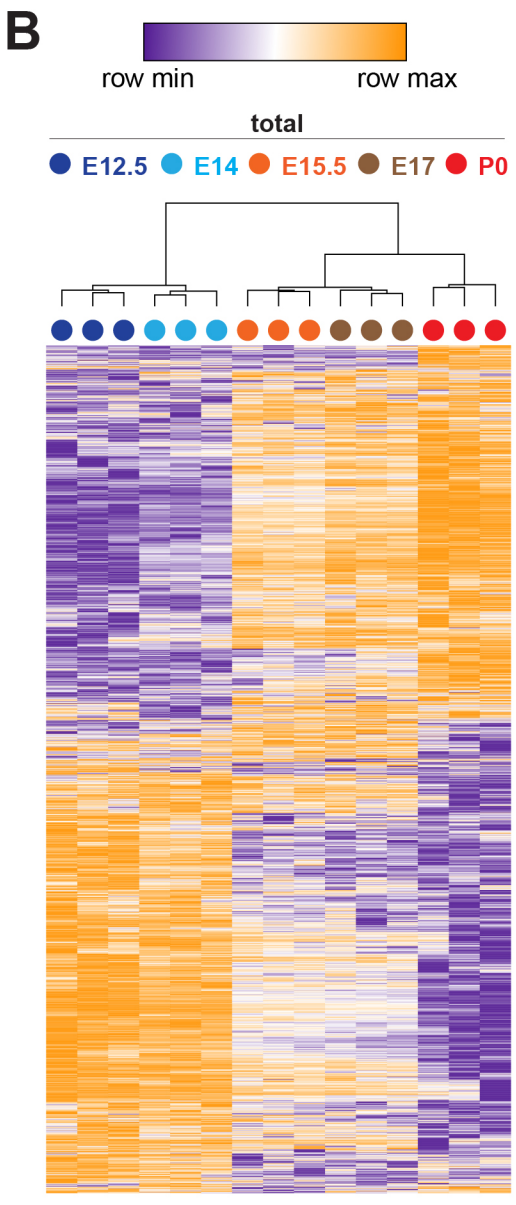

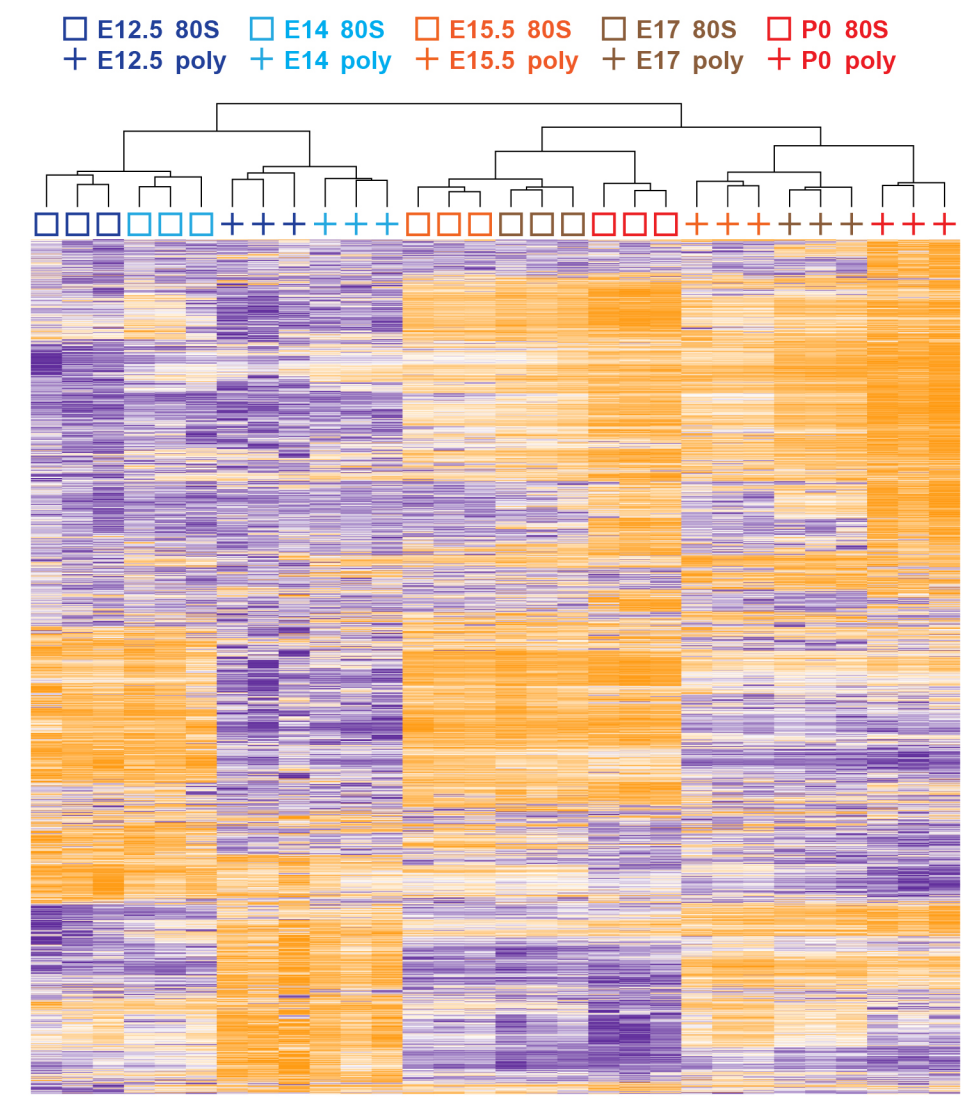

Supplementary Figure 2

Kraushar ML, *et al.*

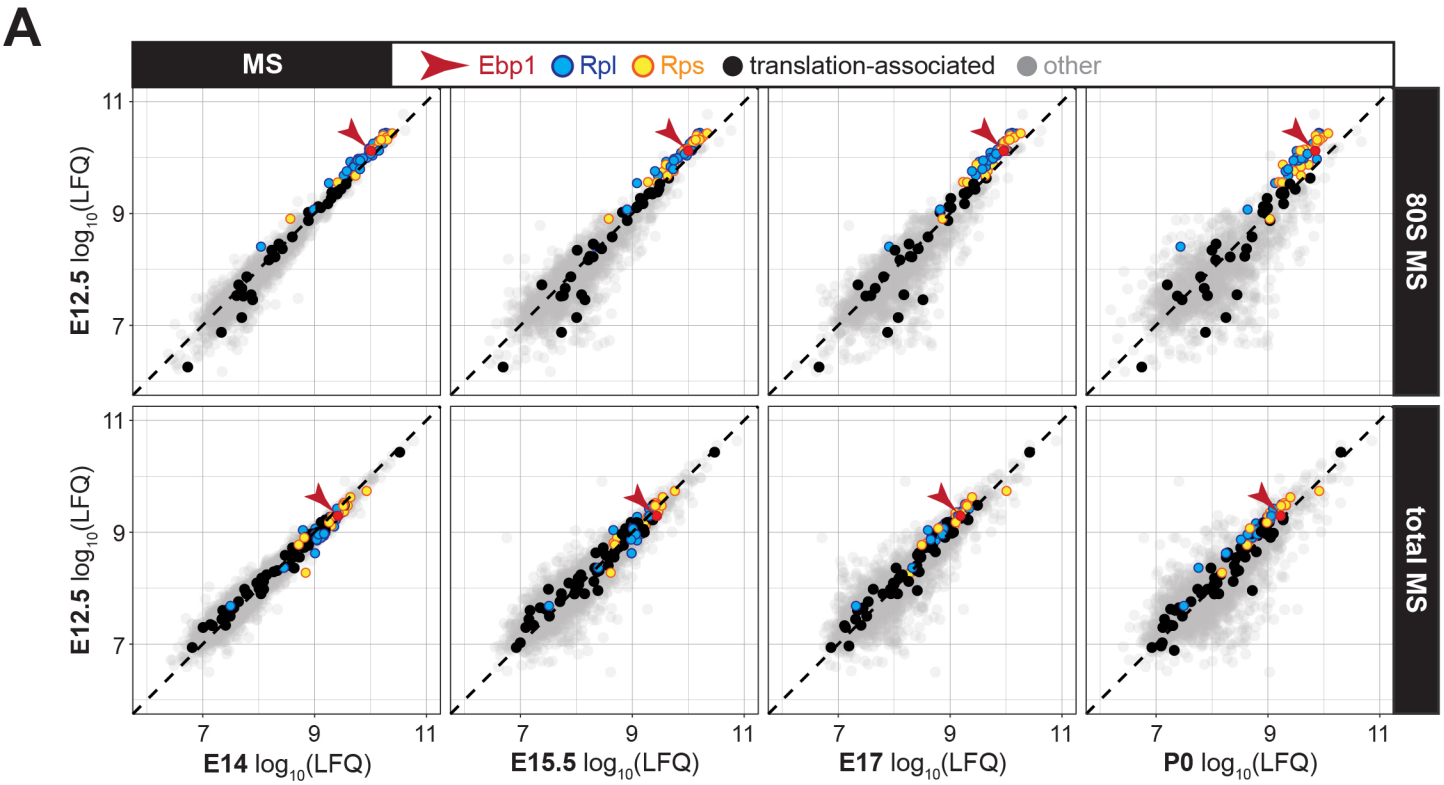

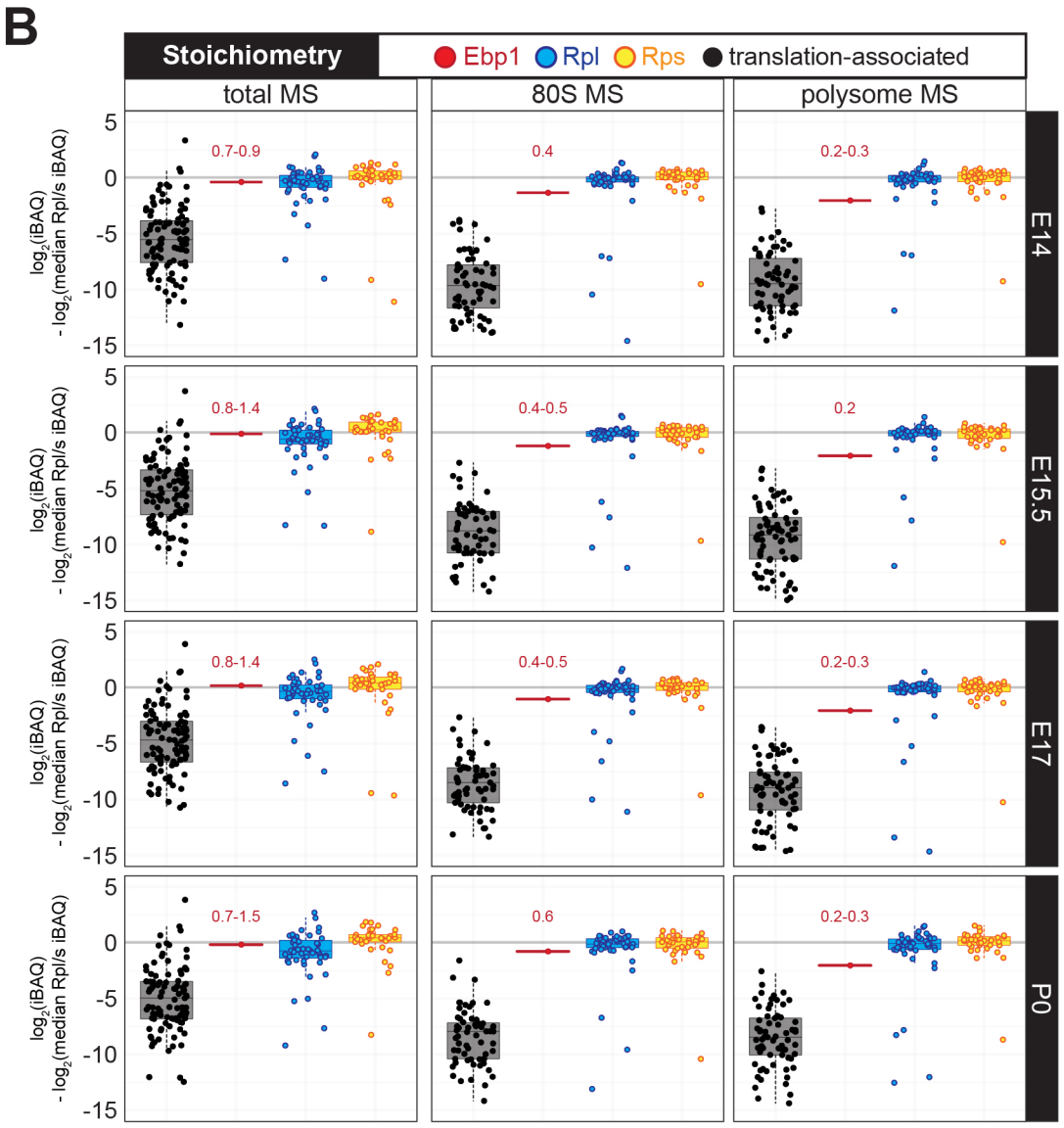

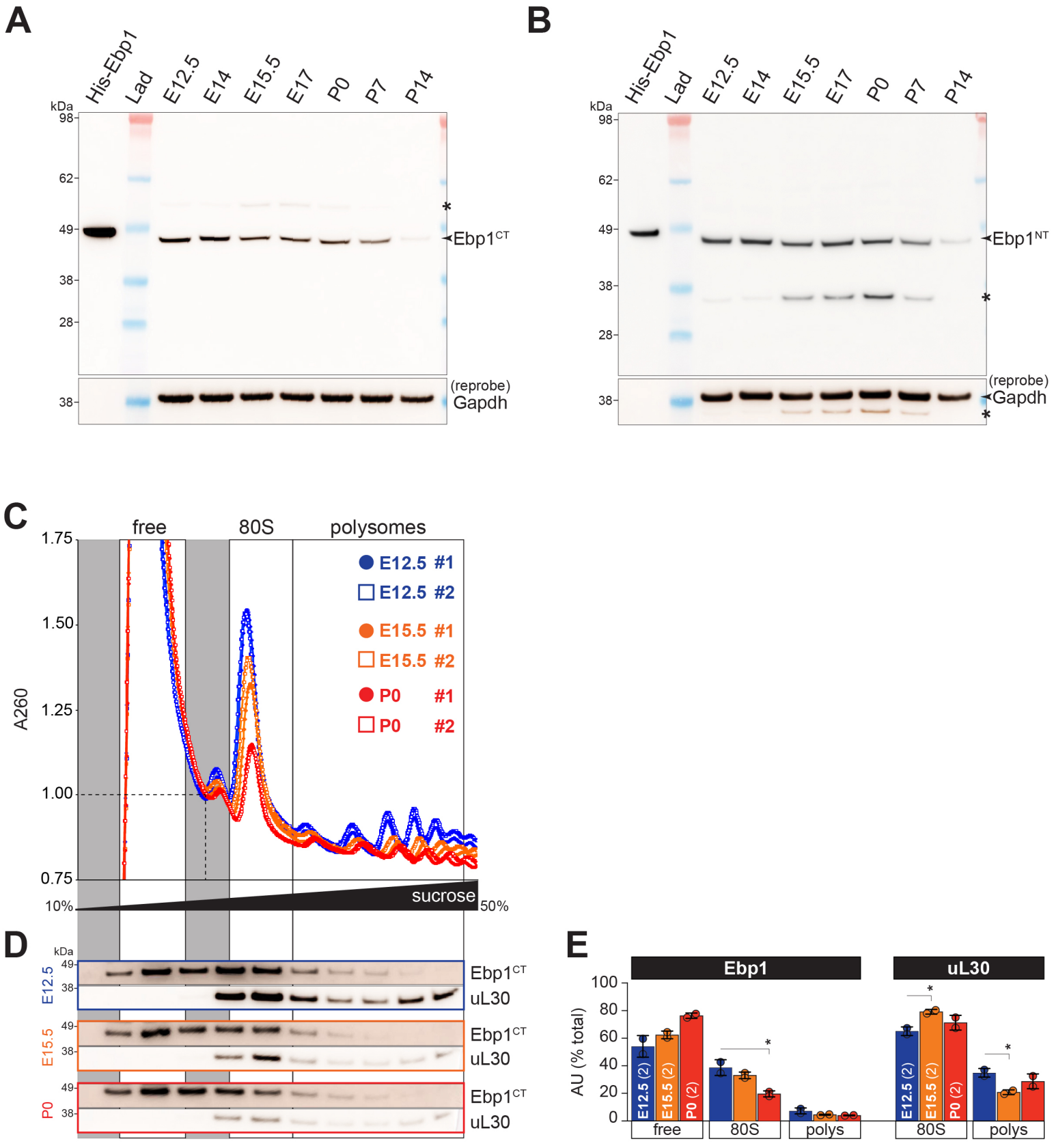
A
His-Ebp1
Lad
E12.5
E14
E15.5
E17
P0
P7
P14
kDa
98
62
49
38
28
Ebp1CT
(reprobe)
Gapdh
B
Ebp1NT
C
free
80S
polysomes
E12.5 #1
E12.5 #2
E15.5 #1
E15.5 #2
P0 #1
P0 #2
A260
1.75
1.50
1.25
1.00
0.75
sucrose
10%
50%
D
E12.5
E15.5
P0
uL30
E
Ebp1
uL30
AU (% total)
100
80
60
40
20
0
E12.5 (2)
E15.5 (2)
P0 (2)
free
80S
polys

Supplementary Figure 4

Kraushar ML, *et al.*

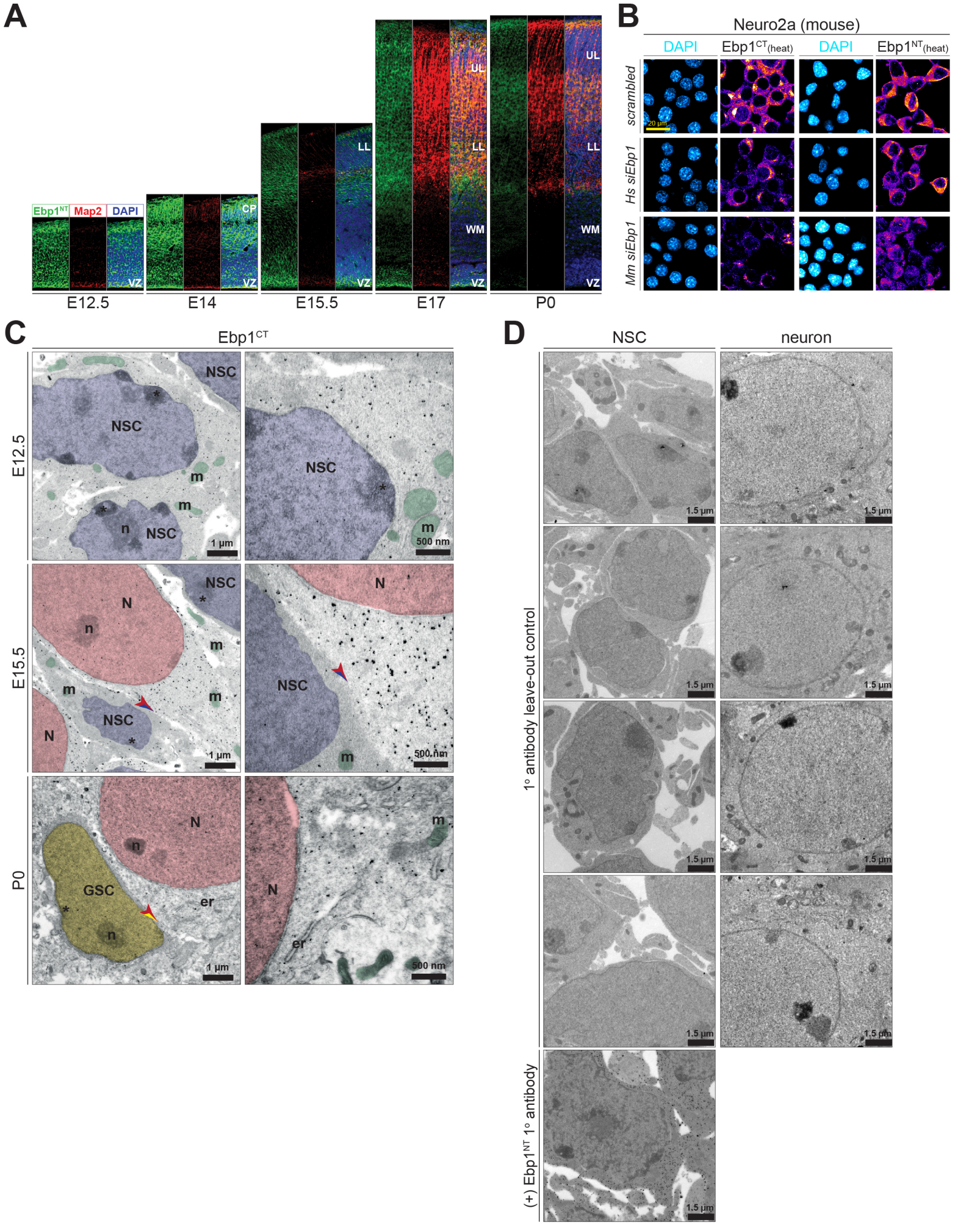

Supplementary Figure 5

Kraushar ML, *et al.*

A

Data collection	
Voltage (keV)	300
Defocus range (μm)	0.5-2.5
Pixel size (Å) on object scale	0.66
Electron dose ($e^-/Å^2$)	31.78

Map refinement				
	Rotated (+)eEF2		*Classical (+)A/A, P/P tRNAs*	
	(+)Ebp1	*(-)Ebp1*	*(+)Ebp1*	*(-)Ebp1*
Particles	23907	29466	15262	14973
Resolution (Å)	3.1	3.1	3.3	3.3

Model	
Composition:	
Chains	58
Atoms	135402 (Hydrogens: 0)
Residues	
Protein	6385
Nucleotide	3887
Water	0
Ligands	
Zn	3
Mg	257
Bonds (RMSD):	
Length Å (# > 4σ)	0.010 (7)
Angles (°) (# > 4σ)	0.702 (45)
MolProbity score	1.47
Clash score	4.06
Ramachandran plot (%)	
Outliers	0.02
Allowed	4.1
Favored	95.89
Rotamer outliers (%)	0.16
Cβ outliers (%)	0
Peptide plane (%)	
Cis proline/general	0.4/0.0
Twisted proline/general	0.4/0.1
CaBLAM outliers (%)	2.74
ADP (B-factors)	
Iso/Aniso (#)	135402/0
min/max/mean	
Protein	43.66/282.25/79.40
Nucleotide	44.27/574.49/99.91
Ligand	29.57/202.48/57.93
Water	---
Occupancy	
Mean	1
occ = 1 (%)	100
0 < occ < 1 (%)	0
occ > 1 (%)	0

Data		
Box		
Lengths (Å)	238.81, 218.91, 270.65	
Angles (°)	90.00, 90.00, 90.00	
Supplied Resolution (Å)	3.3	
Resolution Estimates (Å)	*Masked*	*Unmasked*
d FSC (half maps; 0.143)	---	---
d 99 (full/half1/half2)	3.5/---/---	3.5/---/---
d model	3.4	3.4
d FSC model (0/0.143/0.5)	2.9/3.1/3.3	2.9/3.1/3.6
Map min/max/mean	-10.76/22.03/0.00	

Model vs. Data	
CC (mask)	0.84
CC (box)	0.69
CC (peaks)	0.55
CC (volume)	0.82
Mean CC for ligands	0.75

B

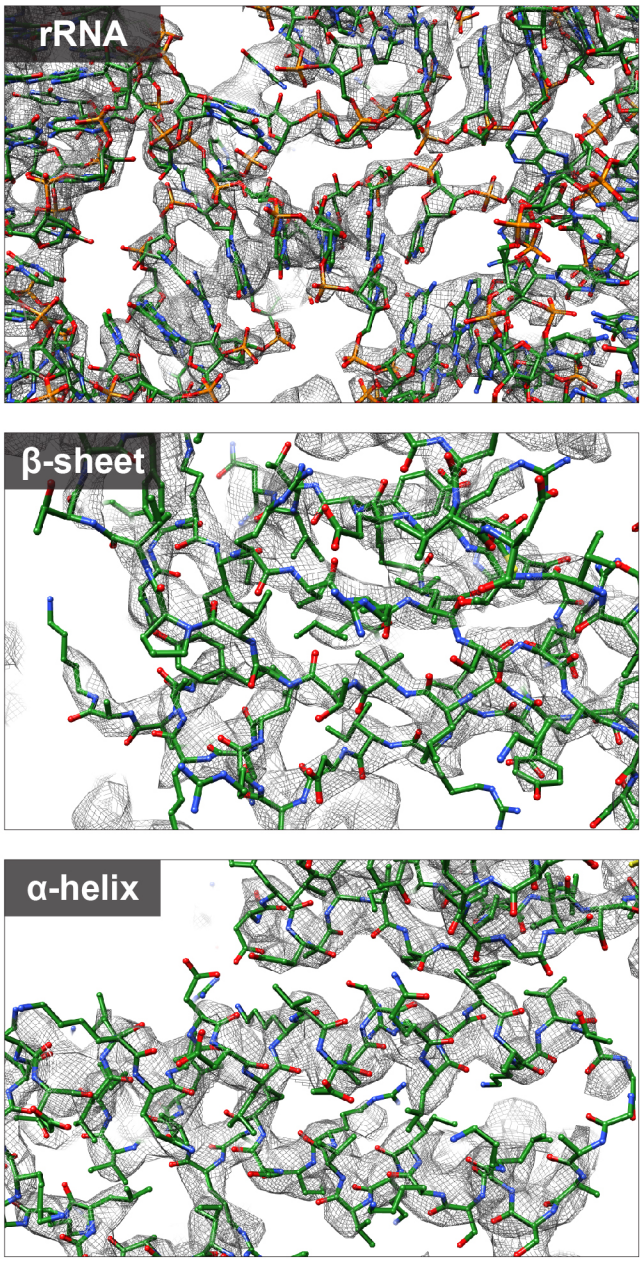

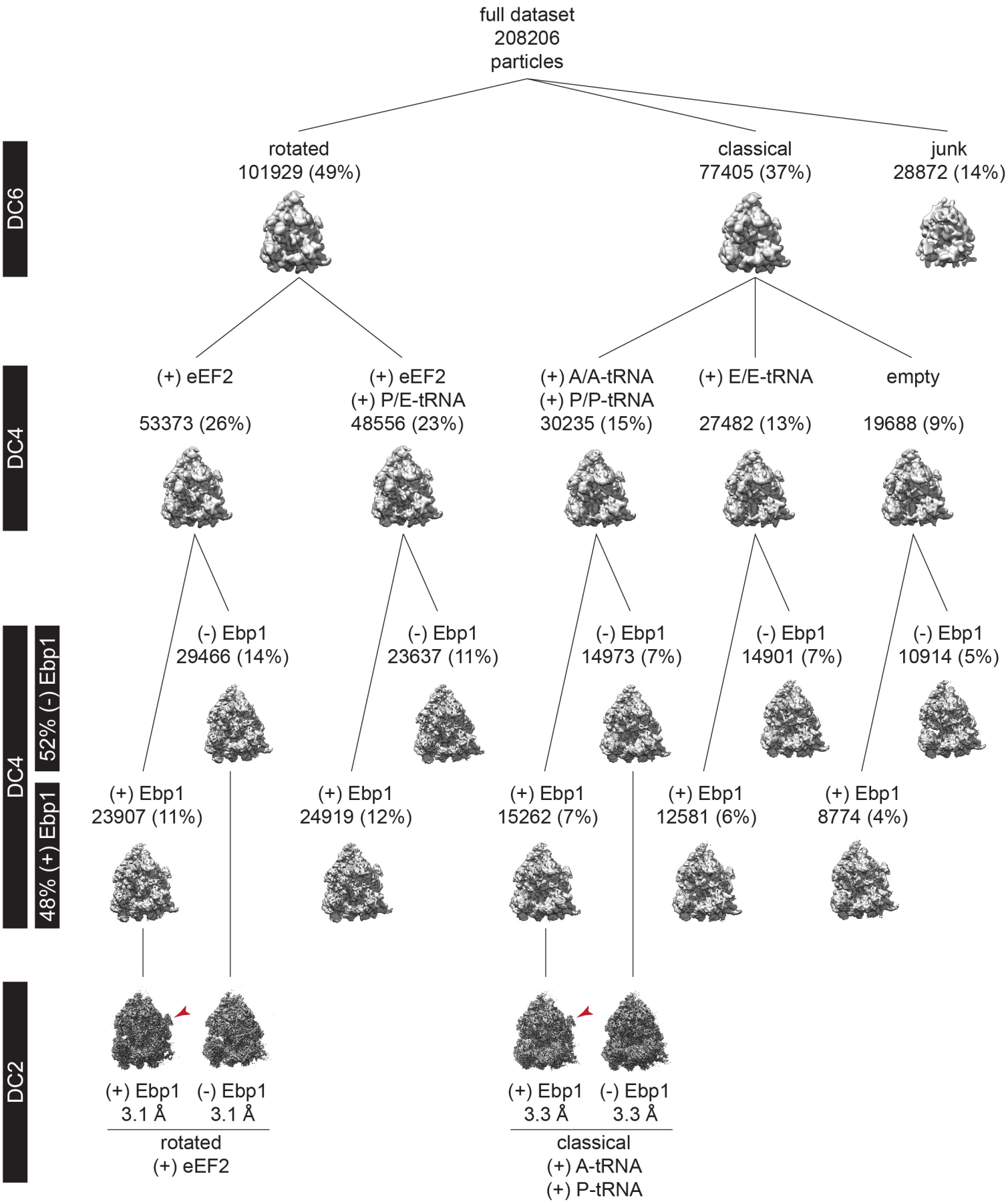
full dataset
208206
particles
DC6
rotated
101929 (49%)
classical
77405 (37%)
junk
28872 (14%)
DC4
(+) eEF2
53373 (26%)
(+) eEF2
(+) P/E-tRNA
48556 (23%)
(+) A/A-tRNA
(+) P/P-tRNA
30235 (15%)
(+) E/E-tRNA
27482 (13%)
empty
19688 (9%)
DC4
52% (-) Ebp1
48% (+) Ebp1
(-) Ebp1
29466 (14%)
(-) Ebp1
23637 (11%)
(-) Ebp1
14973 (7%)
(-) Ebp1
14901 (7%)
(-) Ebp1
10914 (5%)
(+) Ebp1
23907 (11%)
(+) Ebp1
24919 (12%)
(+) Ebp1
15262 (7%)
(+) Ebp1
12581 (6%)
(+) Ebp1
8774 (4%)
DC2
(+) Ebp1
3.1 Å
(-) Ebp1
3.1 Å
rotated
(+) eEF2
(+) Ebp1
3.3 Å
(-) Ebp1
3.3 Å
classical
(+) A-tRNA
(+) P-tRNA

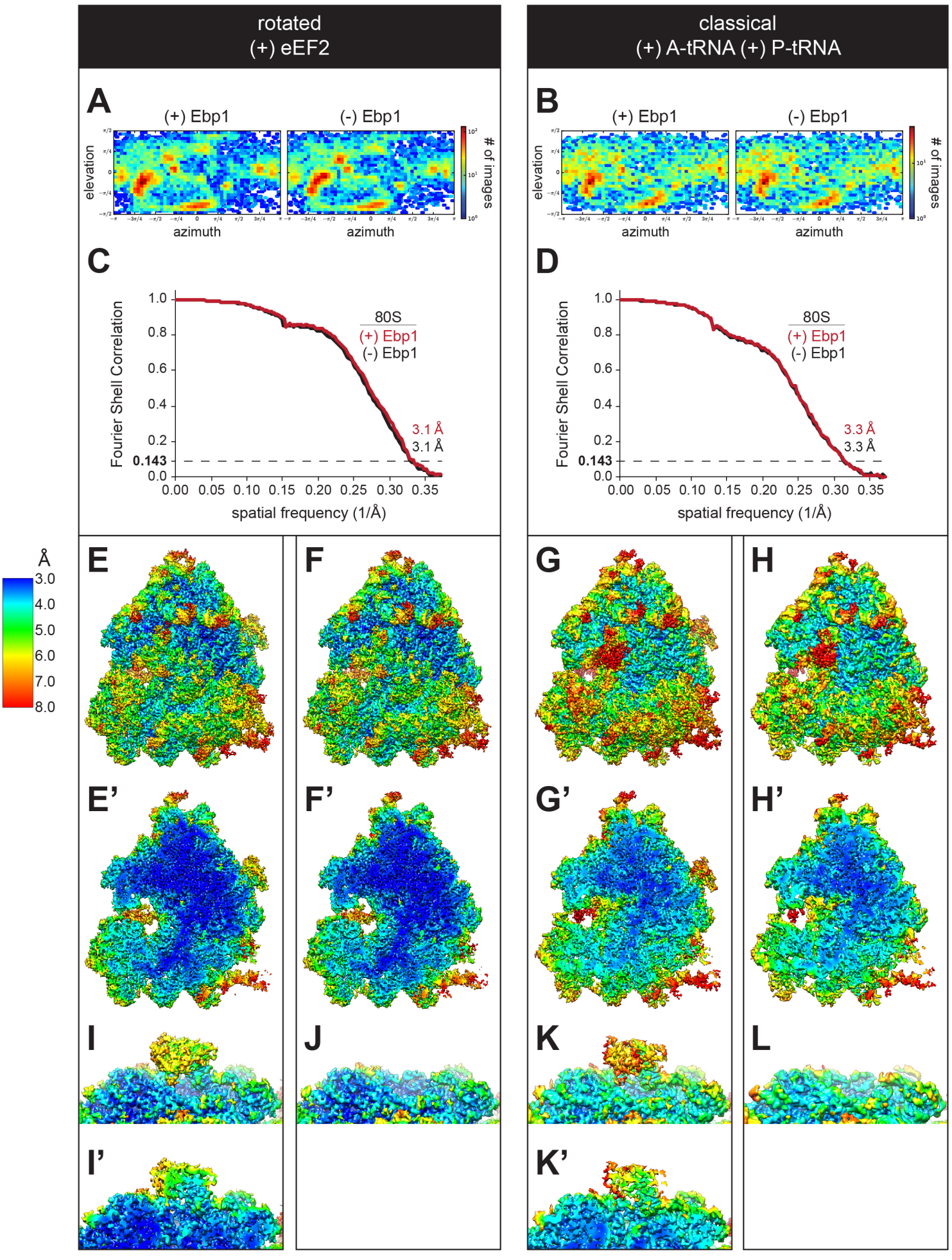
rotated
(+) eEF2
classical
(+) A-tRNA (+) P-tRNA
A
(+) Ebp1
(-) Ebp1
elevation
azimuth
# of images
B
C
Fourier Shell Correlation
80S
(+) Ebp1
(-) Ebp1
3.1 Å
3.1 Å
0.143
spatial frequency (1/Å)
D
3.3 Å
3.3 Å
Å
3.0
4.0
5.0
6.0
7.0
8.0
E
F
G
H
E'
F'
G'
H'
I
J
K
L
I'
K'

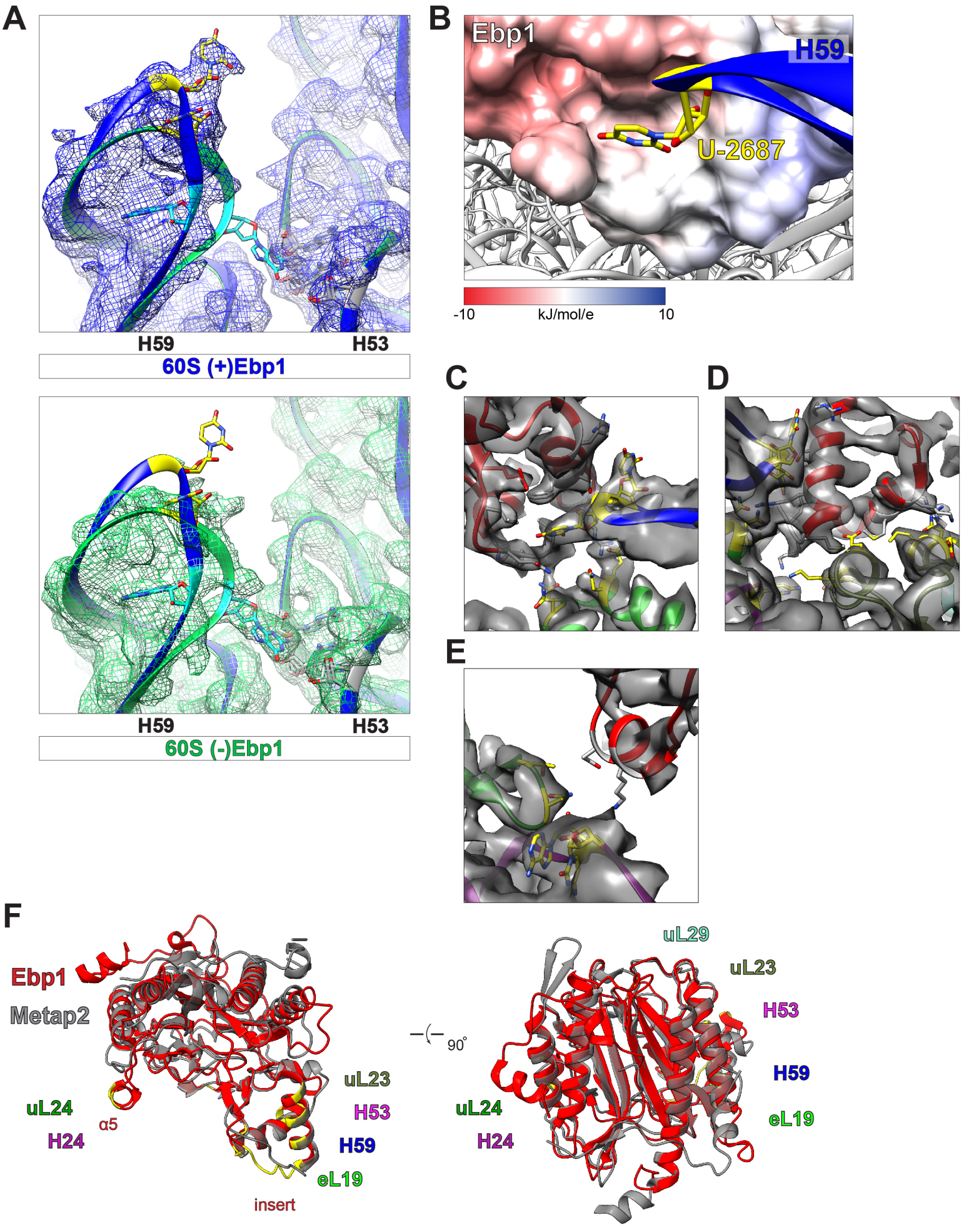
A
H59
H53
60S (+)Ebp1
H59
H53
60S (-)Ebp1
B
Ebp1
H59
U-2687
-10
kJ/mol/e
10
C
D
E
F
Ebp1
Metap2
uL24
H24
α5
uL23
H53
H59
eL19
insert
90˚
uL29
uL23
H53
H59
eL19
uL24
H24

Supplementary Figure 9

Kraushar ML, *et al.*

Supplementary Figure 10

Kraushar ML, *et al*.

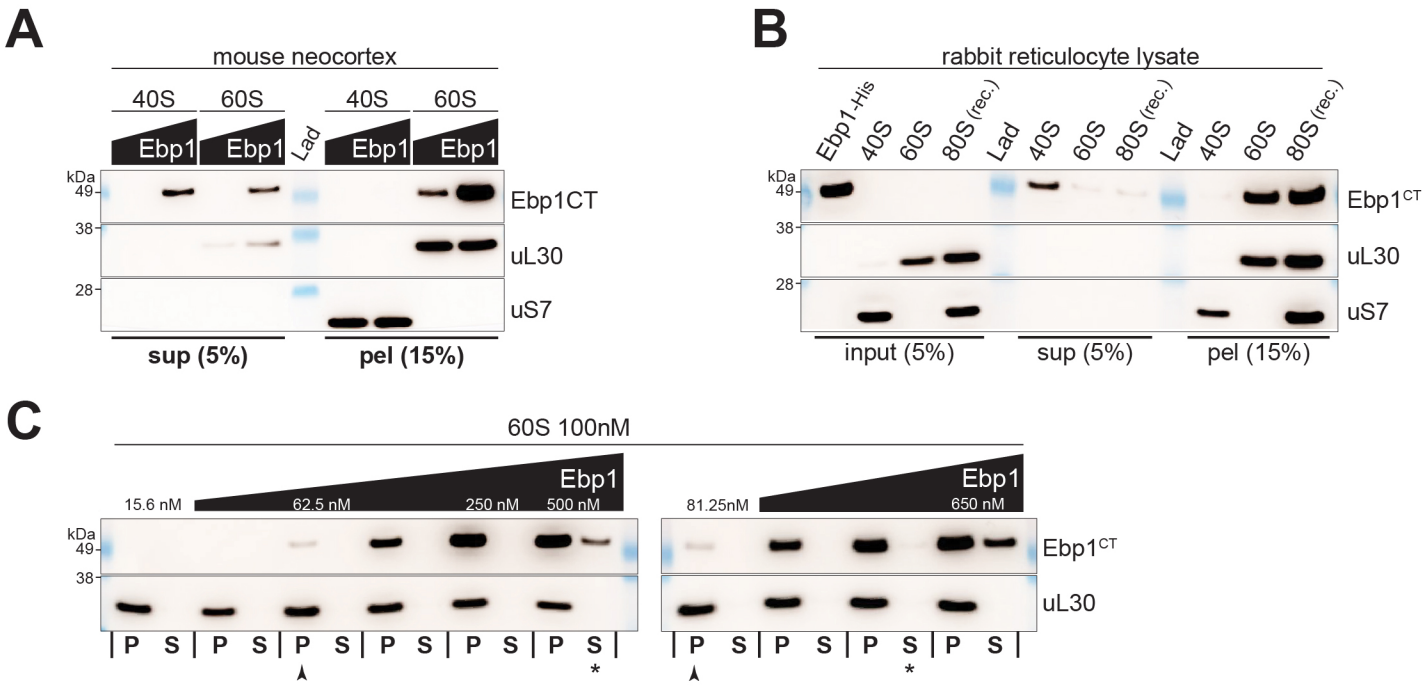

Supplementary Figure 11

Kraushar ML, *et al.*

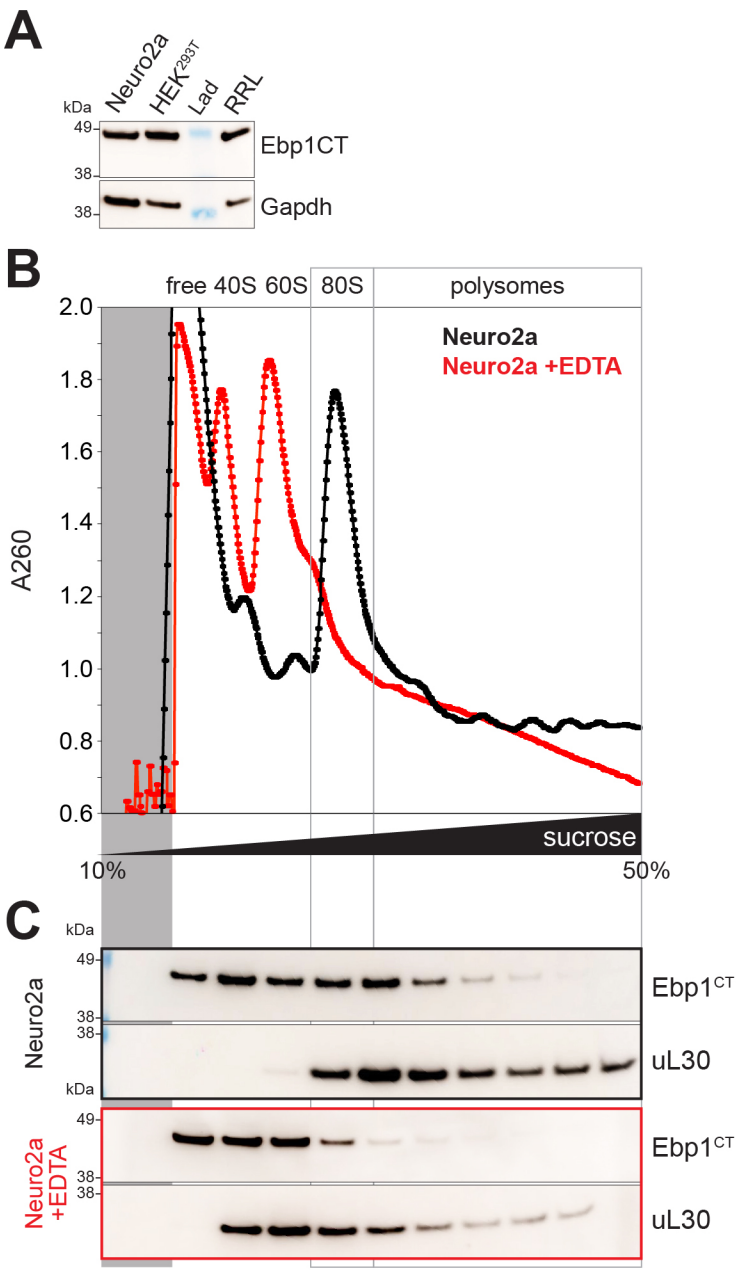

Supplementary Figure 12

Kraushar ML, *et al.*

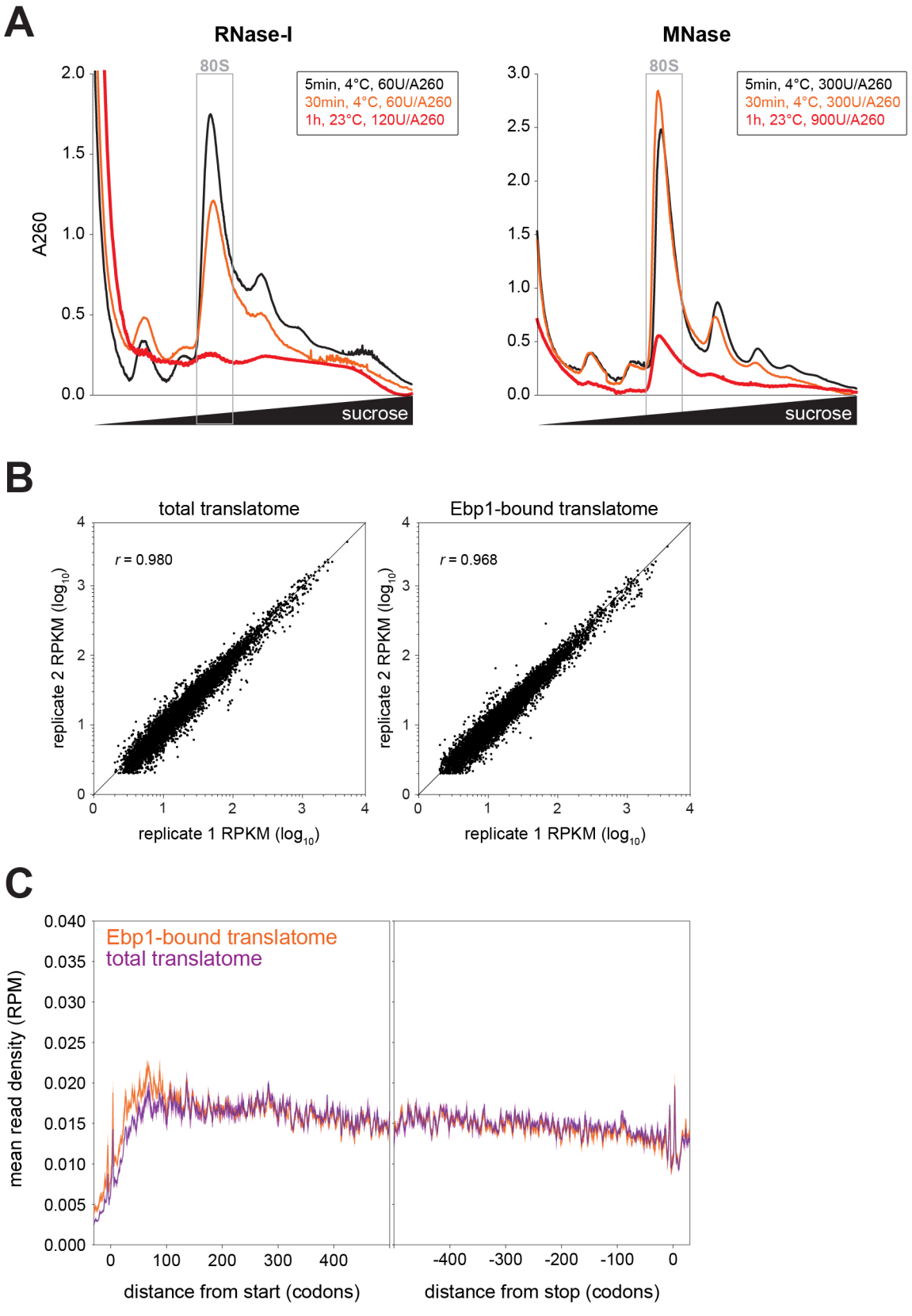

Supplementary Figure 13

Kraushar ML, *et al.*

A

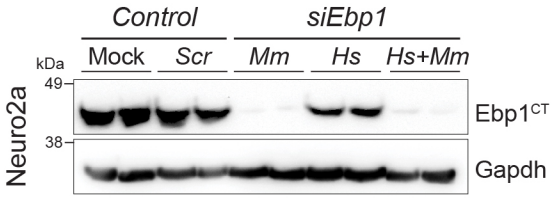

B

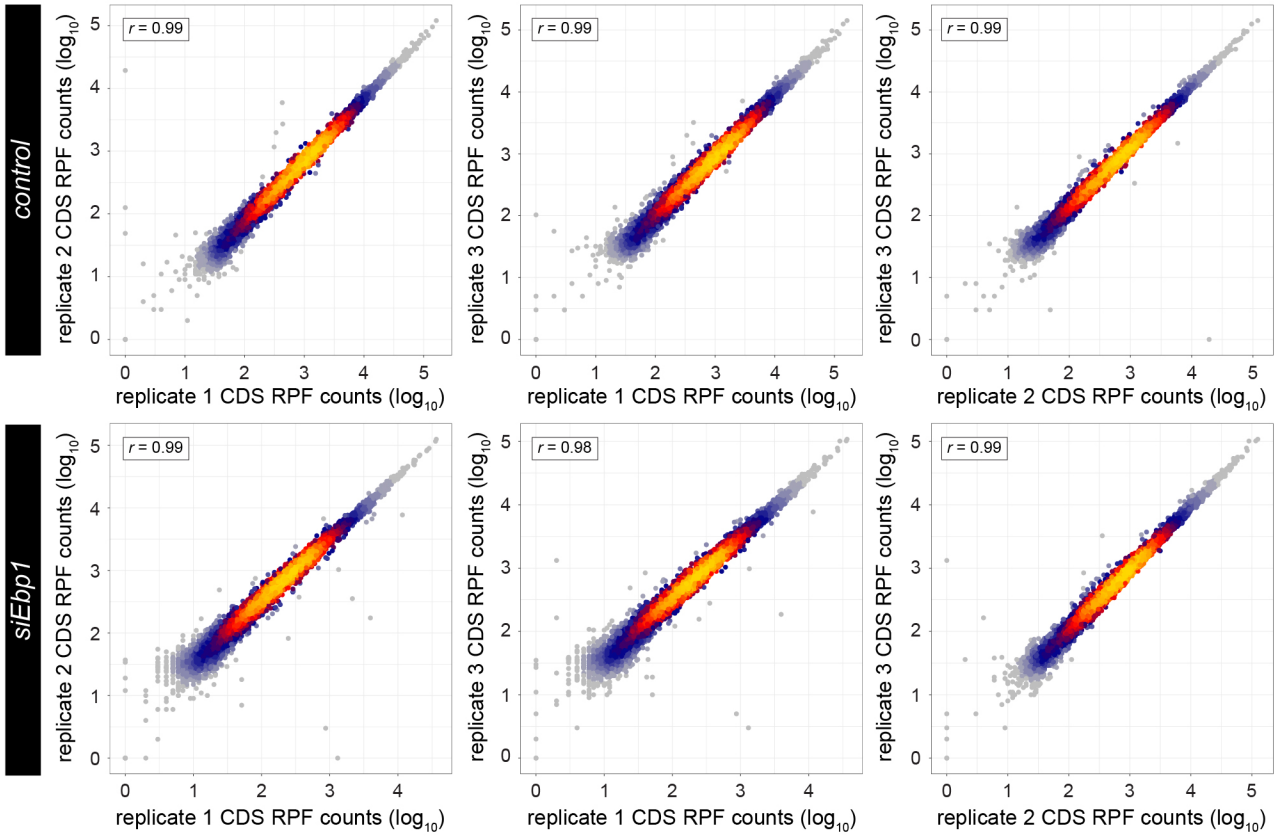

Supplementary Figure 14

Kraushar ML, *et al.*

A

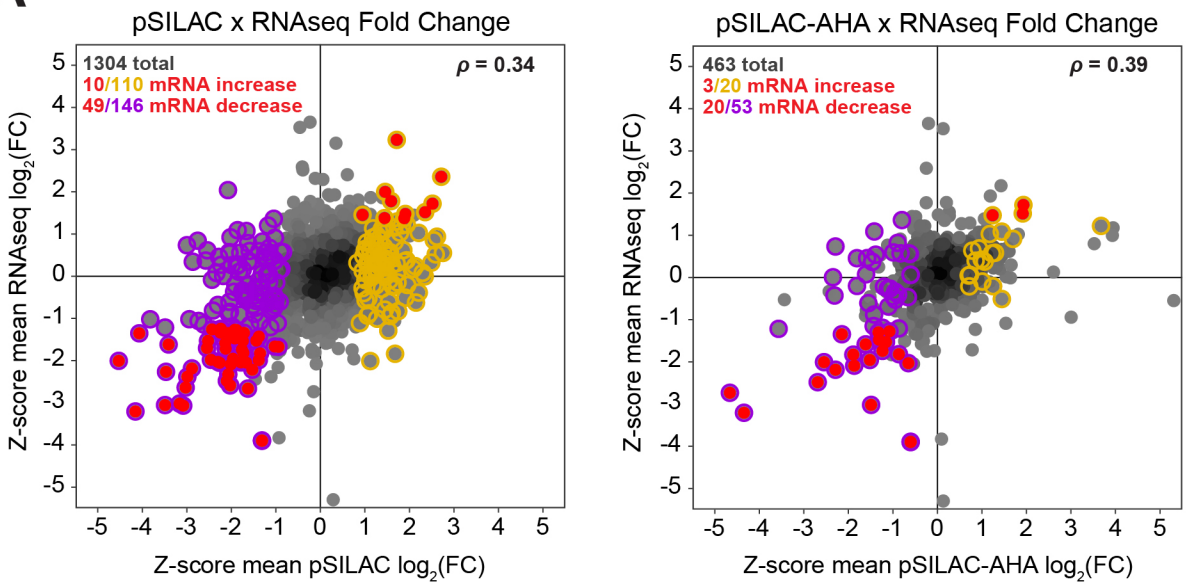

B

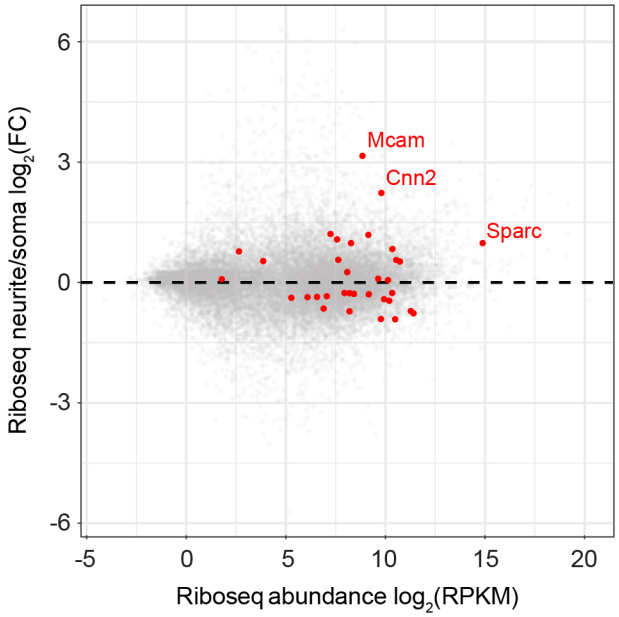

SUPPLEMENTARY FIGURE LEGENDS

Supplementary Figure 1. Hierarchical clustering of MS samples

(A) Mouse neocortical lysates were subjected to preparative sucrose density gradient ultracentrifugation fractionation in biological triplicate to purify 80S and polysomal ribosome complexes at E12.5, E14, E15.5, E17, and P0. Total lysate, pooled 80S fractions, and pooled polysome fractions were analyzed by LC-MS/MS. Hierarchical clustering of neocortex MS data for **(B)** total lysates and **(C)** 80S and polysomes associated with **Figure 1**. Clustering of ANOVA significant (FDR = 0.05) proteins based on one minus Pearson correlation with an average linkage method. Heat maps colored by higher (orange) and lower (purple) protein expression per row (protein ID) max and min, respectively.

Supplementary Figure 2. Total and 80S MS and protein stoichiometry

(A) Scatter plots of protein enrichment in total and 80S MS comparing early neurogenesis E12.5 vs. each subsequent stage. Ebp1, ribosomal proteins of the large (Rpl) and small (Rps) subunits, along with translation-associated proteins are highlighted. Associated with the polysome MS in **Figure 1D**. **(B)** Jitter plots comparing the median stoichiometry of Rpl and Rps (centered at 0) with Ebp1 and translation-associated proteins, in total steady-state, 80S, and polysomes at E14, E15.5, E17, and P0 associated with **Figure 1G**.

Supplementary Figure 3. Total neocortex lysate Western blots, and density gradient fractionation with Western blots associated with Figure 1H

Western blot membranes of total neocortical lysates from E12.5, E14, E15.5, E17, and P0 probed with **(A)** C-terminal specific ($Ebp1^{CT}$, same membrane from **Figure 1F**; Abcam #ab35424) and **(B)** N-terminal specific ($Ebp1^{NT}$, independent replicate from **Figure 1F**; Millipore #ABE43) (Xia et al., 2001) anti-Ebp1, in comparison to full-length recombinant Ebp1 (Ebp1-His). $Ebp1^{CT}$ antibody is expected to identify both full-length Ebp1 ("p48"; ~48kDa, arrows) and a N-terminal truncated isoform ("p42"; ~42kDa), which lacks the first 54 amino acids (Liu et al., 2006). The $Ebp1^{NT}$ antibody should exclusively identify full-length Ebp1. Faint bands are seen at ~55kDa and ~35kDa (stars). Membranes were reprobed with Gapdh as a loading control. We concluded that the starred bands in (A) and (B) are both non-specific signal, since they could not be replicated with both antibodies, and that the dominant isoform of Ebp1 is full-length. Of note, all Ebp1 Western blots in this paper were performed with anti-light chain secondary antibodies, since application of anti-heavy chain secondary was found to introduce strong artifact signal at ~50kDa, creating an obstacle to the interpretation of the 48kDa Ebp1. **(C)** Total

neocortical lysates at E12.5, E15.5, and P0 were A260 normalized, and fractionated by preparative sucrose density gradient ultracentrifugation in biological duplicate, followed by **(D)** Western blot analysis of Ebp1 in each fraction corresponding to extra-ribosomal (free), 80S, and polysomes. uL30 is a marker for ribosome-associated fractions. Individual fractions were pooled to constitute free, 80S, and polysome samples in **Figure 1H**. **(E)** Quantification of (F) (n = 2 blots) of Ebp1 and uL30 levels as a percentage of total signal, mean ± s.d. with t-test for significance. *$p < 0.05$.

Supplementary Figure 4. Ebp1^{NT} immunohistochemistry and Ebp1 immuno-electron microscopy

(A) Ebp1 immunohistochemistry in coronal sections of the developing neocortex with the Ebp1^{NT} antibody, associated with **Figure 2B**. Ventricular zone (VZ), cortical plate (CP), lower layers (LL), and upper layers (UL). Co-immunostaining with Map2, a marker of maturing neurons, along with DAPI labeling nuclei. **(B)** Ebp1 knockdown in mouse Neuro2a cells with siRNA oligos targeting mouse vs. human *Ebp1* mRNA sequences, compared to scrambled siRNA control, followed by immunocytochemistry with Ebp1^{CT} and Ebp1^{NT} antibodies, with the same imaging parameters. While the Ebp1^{NT} antibody yields overall higher signal intensity, loss of signal with knockdown is apparent with both Ebp1^{CT} and Ebp1^{NT} antibodies. Ebp1 protein knockdown in Neuro2a was further confirmed by Western blot (**Figure S13A**) and MS (see **Methods**). **(C)** Immuno-electron microscopy (immuno-EM) with anti-Ebp1^{CT} immunogold labeling (black dots) in the neocortex at E12.5, E15.5, and P0. Neural stem cells (NSC, blue nuclei) and neurons (N, red nuclei). Nucleoli (n), mitochondria (m, green), endoplasmic reticulum (er), cell-cell membrane junctions (arrows). **(D)** Example primary antibody leave-out controls for immuno-EM in **Figures 2C-D**.

Supplementary Figure 5. Cryo-EM data collection and model statistics

(A) Statistics corresponding to cryo-EM data collection, map refinement, model characteristics, data resolution estimation, and cross correlation (CC) of model vs. data associated with **Figures 3-4**. **(B)** Representative cryo-EM map (mesh) to model correspondence for rRNA, β-sheet, and α-helix structures.

Supplementary Figure 6. Multiparticle sorting and refinement of mouse neocortical ribosome states

Cryo-EM imaging of pooled 80S and polysome complexes derived from the P0 mouse neocortex *ex vivo* yielded 208206 particles for *in silico* analysis. Initial multiparticle sorting of

data at six times decimation (DC6) for large-scale heterogeneity generated ribosomes in the rotated and classical states, and a junk population. Further sorting within the rotated and classical states proceeded at DC4. In the rotated state, populations with eEF2 and eEF2+P/E tRNA emerged. In the classical state, populations with A/A+P/P tRNAs, E/E tRNA, and without tRNA emerged. In each of these five populations, extra-ribosomal density was observed at the peptide tunnel exit. Further sorting within each of these five populations proceeded at DC4 with a focus mask applied to this extra-ribosomal density as described in the Methods, to disentangle cofactor-positive and cofactor-negative ribosome sub-states. Each of these five populations yielded cofactor-positive and -negative populations. Final high-resolution refinement at DC2 proceeded for cofactor-positive (red arrow) and -negative populations of the rotated state with eEF2 (3.1Å global resolution), and the classical state with A/A+P/P tRNAs (3.3Å global resolution). These high-resolution data allowed for the identification of the cofactor as Ebp1, with cofactor-positive and -negative sub-states revealing 60S structural changes with Ebp1 binding. See also **Figures 3-4**.

Supplementary Figure 7. Global and local resolution measurements of cryo-EM maps

Particle orientation distribution and global resolution Fourier Shell Correlation (FSC) for the **(A, C)** rotated state with eEF2, and **(B, D)** classical state with A/A+P/P tRNAs, both with and without Ebp1, associated with **Figures 3-4**. Local resolution heat maps for the **(E, E', F, F', I, I', J)** rotated state with eEF2, and **(G, G', H, H', K, K', L)** classical state with A/A+P/P tRNAs, both with (E, E', I, I'; G, G', K, K') and without (F, F', J; H, H', L) Ebp1. Maps are shown in both surface (E, F, G, H, I, J, K, L) and cross-section (E', F', G', H', I', K'). The local resolution of Ebp1 is ~4-6Å.

Supplementary Figure 8. Cryo-EM density, electrostatics, and Metap2 structure associated with the Ebp1•60S model

(A) Cryo-EM density (mesh) for the rotated state with eEF2 in Ebp1-positive (blue) and Ebp1-negative (green) sub-states, associated with **Figure 4A**. Density for base U-2687 (yellow) demonstrates flipping out when Ebp1 is bound, along with flipping in of base G-2690 (cyan), and global reorganization of the H59 tip backbone away from H53. Base G-2690 in the Ebp1-negative state demonstrates density bridging to H53 bases G-2501, G-2502, and C-2513 (grey) to stabilize H59's canonical position. **(B)** Reorientation of H59 U-2687 into a pocket of Ebp1's insert domain, facilitating Ebp1 stabilization on the 60S tunnel exit surface. Ebp1 shown as electrostatic potential map. **(C-E)** Cryo-EM density (grey) corresponding to models in **Figures**

4B-D, respectively. **(F)** Global alignment of Ebp1 (red, PDB 2V6C) and Metap2 (grey, PDB 1KQ9), highlighting structural differences with Ebp1's α5 domain, and overall structural similarity, such as the insert domain. Ebp1 residues making electrostatic interactions (yellow) with 60S TE rRNA helices and proteins are highlighted. See also **Figures 4E-F**.

Supplementary Figure 9. Transcriptional landscape of 60S tunnel exit cofactor expression in the developing neocortex

Expression heat maps from scRNAseq data plotting NSC birthdate (x-axis) and differentiation (y-axis) scores, for the relative enrichment of mRNAs coding for 60S tunnel exit cofactors in the developing neocortex (ribosome-binding subunits shown). In each graph, the early-born apical progenitor (AP) NSC pool is plotted in the bottom left, with their corresponding differentiated lower layer neurons (N4d) in the top left. Late-born NSCs are plotted in the bottom right, with their corresponding differentiated upper layer neurons in the top right. See also **Figures 4H-I**. Data derived from (Telley et al., 2019).

Supplementary Figure 10. Biochemical analysis of Ebp1•ribosome subunit binding

(A) 40S and 60S subunits were purified from P0 mouse neocortex, and reconstituted with recombinant Ebp1-His. Escalating doses of Ebp1 (100nM, 200nM) were mixed with a constant 100nM of each subunit, and pelleted through a sucrose cushion to separate free unbound Ebp1 in the supernatant, vs. Ebp1•subunit complexes in the pellet. Marker for the 60S is uL30, and for 40S is uS7. **(B)** Binding assay for purified rabbit reticulocyte-derived subunits and reconstituted 80S, as in (A) with 200nM Ebp1 combined with 100nM of subunit or 80S. **(C)** Binding affinity of Ebp1-His to 60S measured by pelleting assay and Western blot analysis, in independent replicates. Binding first detected in the pellet (P) marked with an arrow, and excess Ebp1 in the supernatant (S) marked with a star. Associated with **Figure 4J**.

Supplementary Figure 11. Ebp1-ribosome association in Neuro2a cells

(A) Western blot of Neuro2a, HEK-293T, and rabbit reticulocyte (RRL) total lysates probed with $Ebp1^{CT}$ antibody. **(B)** Preparative sucrose density gradient fractionation of Neuro2a cell lysates with and without 100 mM EDTA, followed by **(C)** Western blot analysis of Ebp1 enrichment in each fraction. uL30 is a marker for 60S fractions. Associated with **Figures 5-6**.

Supplementary Figure 12. Ebp1-selective ribosome profiling

(A) RNase titration with RNase-I and MNase in Neuro2a lysates, followed by sucrose density gradient fractionation for measurement of 80S monosome enrichment. As previously described for mouse tissue lysates (Gerashchenko and Gladyshev, 2017), we observed both monosome and polysome degradation with RNase-I digestion, which may compromise the quality of ribosome immunoprecipitation (IP) for selective ribosome profiling. In contrast, MNase digestion decreased polysome enrichment with a concomitant increase in monosomes, and was utilized for this experiment. **(B)** Correlation of biological replicates (*n* = 2) in Ebp1-selective ribosome profiling. **(C)** Center-weighted metagene profiles of Ebp1-IP and total translatomes near the start and stop codon, demonstrating enrichment in the CDS. Of note, MNase digestion has been previously reported to generate more ribosome-protected fragments within the 3'-UTR (Miettinen and Björklund, 2015). See also **Figures 5A-F**.

Supplementary Figure 13. Ebp1-knockdown ribosome profiling

(A) Western blot analysis of Ebp1 knockdown in mouse Neuro2a cells with siRNA oligos targeting mouse vs. human *Ebp1* mRNA sequences, compared to mock transfection and scrambled siRNA controls, in biological duplicate. **(B)** Correlation of biological replicates (*n* = 3) in Ebp1-knockdown ribosome profiling. See also **Figures 5G-I**.

Supplementary Figure 14. Correlation of Ebp1-knockdown pSILAC/AHA MS with Ebp1-knockdown RNAseq, and neurite vs. soma ribosome profiling

(A) Correlation between pSILAC (left figure) and pSILAC-AHA (right figure) MS fold change (**Figure 6E**), and the RNAseq fold change (**Figures 5G-I**), of Ebp1 knockdown/control per gene in Neuro2a cells. Z-scored fold change is plotted to account for variability in mRNA and pSILAC measurements. Shown in yellow and purple are all genes with levels found up and down (≥ 1.25-fold change), respectively, in the pSILAC and pSILAC-AHA analysis alone (note: this is a lower number than the reported values in **Figure 6E**, as expected, because some peptides are not confidently matched to unique mRNA annotations). Highlighted in red are those proteins with commensurate changes in mRNA levels (ratios shown at top left). Of note, some proteins with decreased/increased synthesis also show mRNA changes in the opposite direction. **(B)** Ribosome profiling data derived from (Zappulo et al., 2017), highlighting the relative enrichment of Ebp1-regulated proteins (red, ≥ 2-fold change vs. control, **Figure 6E**) in soma vs. neurite localized (y-axis) protein synthesis compared the mRNA RPKM (x-axis) of cultured neurons.